Nano Research 2015, 8(2): 576–583
DOI 10.1007/s12274-014-0689-3
Research Article
ISSN 1998-0124
CN 11-5974/O4

Hierarchical Co_3O_4 porous nanowires as an efficient bifunctional cathode catalyst for long life Li–O_2 batteries

Qingchao Liu[1,2], Yinshan Jiang[2], Jijing Xu[1], Dan Xu[1], Zhiwen Chang[1,3], Yanbin Yin[1,2], Wanqiang Liu[4], and Xinbo Zhang[1] (✉)

[1] *State Key Laboratory of Rare Earth Resource Utilization, Changchun Institute of Applied Chemistry, Chinese Academy of Sciences, Changchun 130022, China*
[2] *School of Materials Science and Engineering, Jilin University, Changchun 130012, China*
[3] *Graduate University of Chinese Academy of Sciences, Beijing 100049, China*
[4] *School of Materials Science and Engineering, Changchun University of Science and Technology, Changchun 130022, China*

Received: 9 September 2014
Revised: 9 December 2014
Accepted: 10 December 2014

KEYWORDS
lithium–oxygen batteries,
bifunctional cathode catalyst,
Co_3O_4 nanowires,
cycling stability

ABSTRACT

Hierarchical Co_3O_4 porous nanowires (NWs) have been synthesized using a hydrothermal method followed by calcination. When employed as a cathode catalyst in non-aqueous Li–oxygen batteries, the Co_3O_4 NWs effectively improve both the round-trip efficiency and cycling stability, which can be attributed to the high catalytic activities of Co_3O_4 NWs for the oxygen reduction reaction and the oxygen evolution reaction during discharge and charge processes, respectively.

1 Introduction

Rechargeable nonaqueous lithium–oxygen (Li–O_2) batteries have been attracting intensive interest due to their exceptionally high energy density of 3,600 Wh·kg^{-1} according to the electrochemical reaction ($2Li + O_2 + 2e^- \rightleftharpoons Li_2O_2$, 2.96 V vs. Li/Li$^+$), which is nearly 10 times that of conventional lithium-ion batteries [1–4]. This high energy density endows Li–O_2 batteries with great promise in electric vehicles and large scale renewable energy storage. However, the terribly sluggish oxygen reduction reaction (ORR) and oxygen evolution reaction (OER) kinetics not only increase the overpotential, but also cause poor rate capability of Li–O_2 batteries. Besides, the insoluble discharge products formed on the cathode during the discharge process easily block the transfer channels of electrolyte and oxygen, inevitably leading to short cycle life [5–7]. Electrocatalysts

Address correspondence to xbzhang@ciac.ac.cn

are thus necessary to alleviate the sluggish ORR and OER kinetics and the blockage of cathode channels caused by Li_2O_2 aggregation, in order to improve the round-trip efficiency and cycling life Li–O_2 batteries.

Up to now, carbon supported transition metal oxides, such as Fe_2O_3, Co_3O_4, MnO_2 and their composite oxides have been widely investigated as electrocatalysts for nonaqueous Li–O_2 batteries [8–14]. Among them, Co_3O_4 exhibits superior activity towards ORR and OER compared with other transition metal oxides. Various morphologies of Co_3O_4 have been synthesized and employed in energy storage systems, and the electrochemical performance was found to be significantly influenced by the morphology [15–19]. However, the effect of the electrochemical performance derived from designed Co_3O_4 morphology and its structure-activity on the Li–O_2 battery cathode structure has been rarely reported [20–23]. Herein, high surface area Co_3O_4 nanowires (NWs) with a chrysanthemum-like structure composed of porous NWs have been synthesized using a hydrothermal method followed by calcination. Benefiting from the large number of catalyst sites and the effectively tailored cathode structure, the Li–O_2 battery with the Co_3O_4 NWs exhibits excellent round-trip efficiency and cycling life.

2 Experimental

2.1 Materials synthesis

In a typical experiment, 5 mmol of $Co(NO_3)_2$ and 3 mmol of urea as well as 1 mmol of $(NH_4)_2S_2O_8$ were dissolved in 40 mL of deionized water. After stirring for several minutes, the solution was transferred to 50 mL Teflon-lined stainless steel autoclave and then hydrothermally treated at 180 ℃ for 12 h in an electric oven. After the treatment, the pink precipitate was collected by centrifugation, washed three times with water and ethanol, and then dried in an oven. This precursor powder was then thermally decomposed at 350 ℃ for 2 h.

2.2 Materials characterization

Samples for scanning electron microscopy (SEM) were prepared by directing putting the electrode sample onto to a SEM brass stub. Transmission electron microscopy (TEM) was performed using a FEI Tecnai G2 S-Twin instrument with a field emission gun operating at 200 kV. Samples dispersed in ethanol were applied onto the Cu grid with carbon coated on a lacey support film and dried in air before TEM imaging. Powder X-ray diffraction (XRD) measurements were performed on a Bruker D8 focus power X-ray diffractometer with Cu Kα radiation (λ = 1.5405 Å). Nitrogen adsorption–desorption measurements were performed on a Micromeritics ASAP2020 adsorption analyzer. Specific surface areas were calculated by the Brunauer–Emmett–Teller method. Pore volumes and sizes were estimated from the pore-size distribution curves from the adsorption isotherms using the Barrett–Joyner–Halenda method. Electrochemical impedance spectroscopy (EIS) measurements and cyclic voltammograms (CV) were performed on a BioLogic VMP3 electrochemical workstation. Li–O_2 battery measurements were cycled on a LAND CT 2001A multichannel battery testing system.

2.3 Cell assembly

CR2032-type cells were used in this study. For the cathode, a slurry was prepared by mixing carbon black–Super-P (SP, 60 wt.%), Co_3O_4 NWs or Co_3O_4 NPs (30 wt.%) and lithium-exchanged Nafion binder (10 wt.%). For comparison, SP as a cathode was also tested. All the cells were assembled under an argon atmosphere, using a clean lithium metal disk as the anode, a glass-fiber separator, and a 1 M tetraethylene glycol dimethyl ether (TEGDME)–lithium trifluoromethane sulfonate ($LiCF_3SO_3$) electrolyte. The gravimetric capacity was calculated based on the carbon mass.

3 Results and discussion

The morphology of the precursor and Co_3O_4 NWs was investigated by SEM and TEM techniques. Figure 1(a) presents a typical SEM image of the Co_3O_4 NWs. The product has a chrysanthemum-like architecture composed of porous NWs, indicating that the morphology remains unchanged during the thermal decomposition process of the precursor (Fig. S1 in the Electronic Supplementary Material (ESM)). The NWs

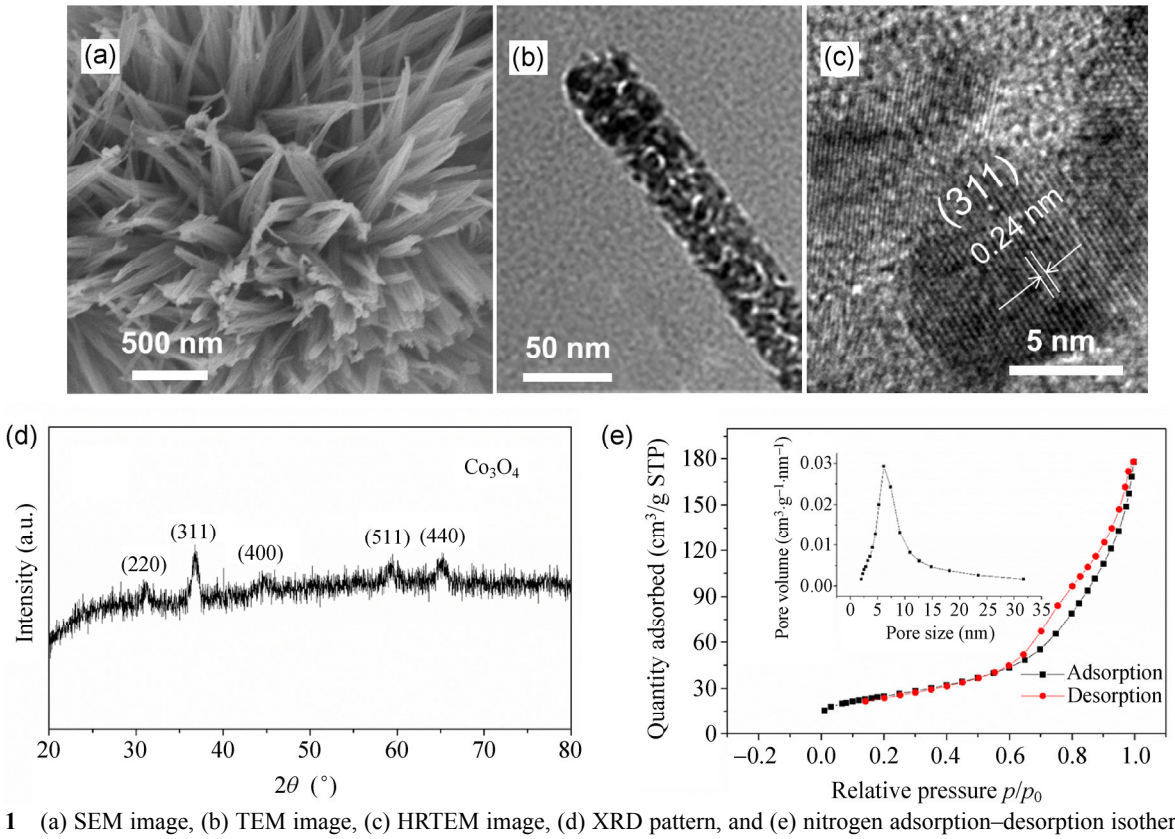

Figure 1 (a) SEM image, (b) TEM image, (c) HRTEM image, (d) XRD pattern, and (e) nitrogen adsorption–desorption isotherms and pore-size distribution curve (inset) of the obtained porous Co_3O_4 NWs.

are ca. 30 nm in width, and are composed of interconnected NPs with a size of ca. 5 nm (Fig. 1(b)). A high-resolution TEM (HRTEM) image (Fig. 1(c)) shows lattice fringes with a spacing of 0.24 nm, corresponding to the (311) planes of the spinel Co_3O_4, which is consistent with the XRD pattern (Fig. 1(d)) (space group: $Fd\bar{3}m$ (No. 227), JCPDS card No. 42-1467). As shown in Fig. 1(e), the N_2 adsorption–desorption isotherms and pore-size distribution data show that the specific surface area and the size of the pores of Co_3O_4 NWs is 87.47 $m^2 \cdot g^{-1}$ and 5–10 nm, respectively. For comparison, the Co_3O_4 NPs with size ca. 100 nm were also synthesized [24] (Fig. S3 in the ESM), and their specific surface area is ca. 27.91 $m^2 \cdot g^{-1}$ (Fig. S4 in the ESM).

Figure 2(a) shows the first discharge–charge curves of three different Li–O_2 cells with SP, Co_3O_4 NWs/SP, and Co_3O_4 NPs/SP cathodes with a fixed capacity of 1,000 $mA \cdot h \cdot g^{-1}$ at a current density of 200 $mA \cdot g^{-1}$. Interestingly, the charge potential of cells with either Co_3O_4 NWs/SP or Co_3O_4 NPs/SP cathodes were both lower than cells containing the pure SP cathode in the initial cycle. The lower potential may arise from the catalytic activity of Co_3O_4 and the variation of Li_2O_2 state caused by catalyst addition (vide infra) [25, 26]. In order to investigate the catalytic activity of Co_3O_4 NWs/NPs, artificial Li–O_2 cells with 0.5 mg of commercial Li_2O_2 were assembled and then charged with capacity restricted to 1,000 $mA \cdot h \cdot g^{-1}$ (based on carbon mass) (Fig. 2(b)). Similarly, it was found that the charge potentials of cells with Co_3O_4 NWs/SP and Co_3O_4 NPs/SP were much lower than a cell with pure SP by about 60 mV, which further demonstrates the efficient OER catalytic performance of Co_3O_4. Cyclic voltammograms (CV) of Li–O_2 cells with pure SP, Co_3O_4 NPs/SP and Co_3O_4 NWs/SP cathodes were recorded at a scan rate of 0.05 $mV \cdot s^{-1}$ (Fig. 2(c)). In the cathodic scan, the cathodic onset potential Li–O_2 cells with Co_3O_4 NPs/SP or Co_3O_4 NWs/SP cathodes were both higher than that with the SP cathode, indicating that Co_3O_4 NPs/SP and Co_3O_4 NWs have better ORR catalytic activity. In the anodic scan, the characteristic features of OER can be observed in all three samples. It should be noted that the Li–O_2 cells with Co_3O_4

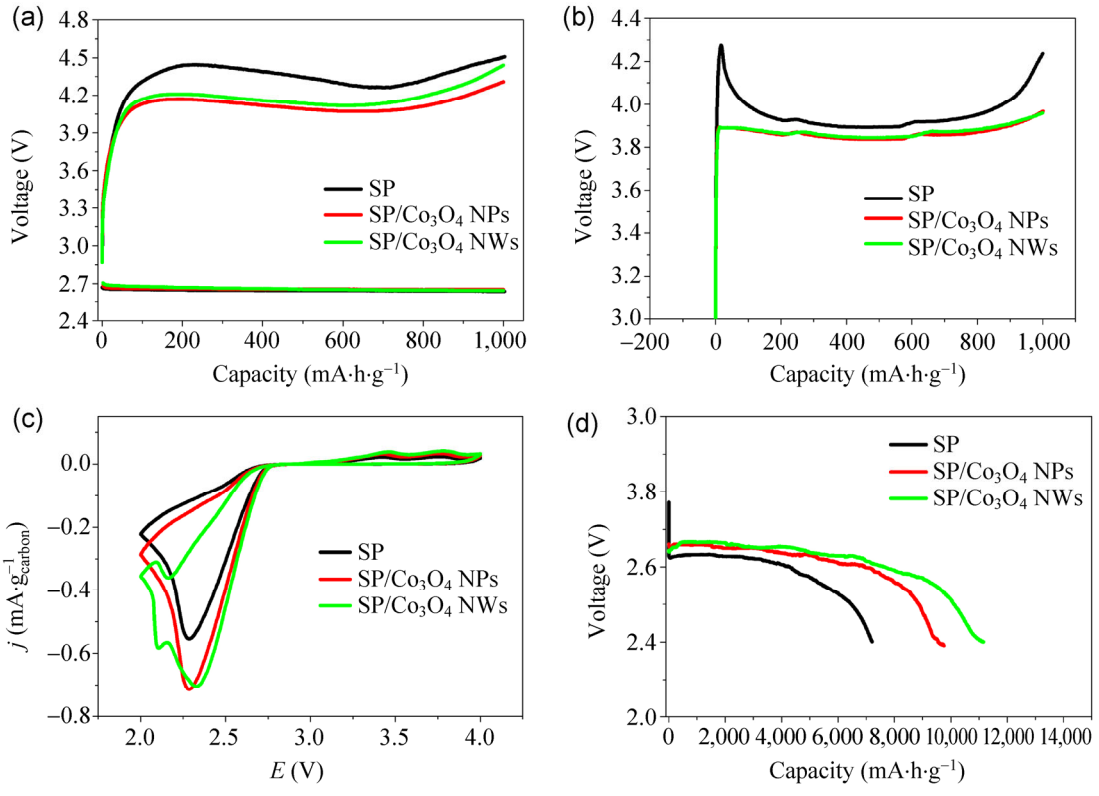

Figure 2 (a) First discharge–charge curves of Li–O_2 cells with a fixed capacity; (b) charge curves of artificial Li–O_2 cells with commercial Li_2O_2; (c) cyclic voltammograms of the Li–O_2 cells with SP, Co_3O_4 NWs/SP or Co_3O_4 NPs/SP cathodes; and (d) the first full discharge curves of the Li–O_2 cells with CP, SP, Co_3O_4 NWs/SP or Co_3O_4 NPs/SP cathodes.

NPs/SP or Co_3O_4 NWs/SP both present lower onset potentials than that of SP, which further demonstrates that the Co_3O_4 NPs/SP and Co_3O_4 NWs/SP have higher OER electrocatalytic activity.

As shown in Fig. 2(d), at a current density of 100 mA·g^{-1} with a cut-off voltage of 2.4 V, the first full discharge capacities of the Li–O_2 cells with SP, Co_3O_4 NPs/SP, and Co_3O_4 NWs/SP cathode were 7,205.8, 9,764.7, and 11,160.8 mA·h·g^{-1}, respectively. The efficient ORR catalytic activity of Co_3O_4 could be responsible for the higher discharge capacity of Li–O_2 cells with Co_3O_4 NPs or NWs. Furthermore, the fact that the discharge capacity of the cell with Co_3O_4 NWs/SP is higher than that with Co_3O_4 NPs/SP can be attributed to the higher surface area of Co_3O_4 NWs. Inspired by the high discharge capacity, the rate performance of the cell with a Co_3O_4 NWs/SP cathode was then tested under different current densities with a cut-off voltage of 2.2 V. As shown in Fig. S6 in the ESM, high capacities of 12,629 and 5,516.6 mA·h·g^{-1} can be reached even at current densities of 100 and 500 mA·g^{-1}, respectively, demonstrating that the Co_3O_4 NWs/SP cathode endows the Li–O_2 cell with superior rate capability. Electrochemical impedance spectra were then employed to investigate the reversibility of Li–O_2 cells with SP, Co_3O_4 NWs/SP or Co_3O_4 NPs/SP cathodes. As shown in Fig. S5 in the ESM, after recharging the impedance of all the cells almost returns to the initial value, indicating that the discharge product formed at the cathode during discharge can be decomposed during the subsequent charge process, highlighting the excellent rechargeability of the three cathodes.

The cycling performance of Li–O_2 cells with SP, Co_3O_4 NPs/SP, and Co_3O_4 NWs/SP cathodes was then investigated. As shown in Fig. 3, the cells were tested by controlling discharge depth to 1,000 mA·h·g^{-1} at a current density of 100 mA·g^{-1}. Figures 3(a), 3(c), and 3(e) show the discharge–charge curves of the three cells. Their corresponding cut-off voltages are given in Figs. 3(b), 3(d), and 3(f). Interestingly, it is found that, compared to that with SP (32 cycles), the addition of Co_3O_4 NPs (61 cycles) and especially Co_3O_4 NWs

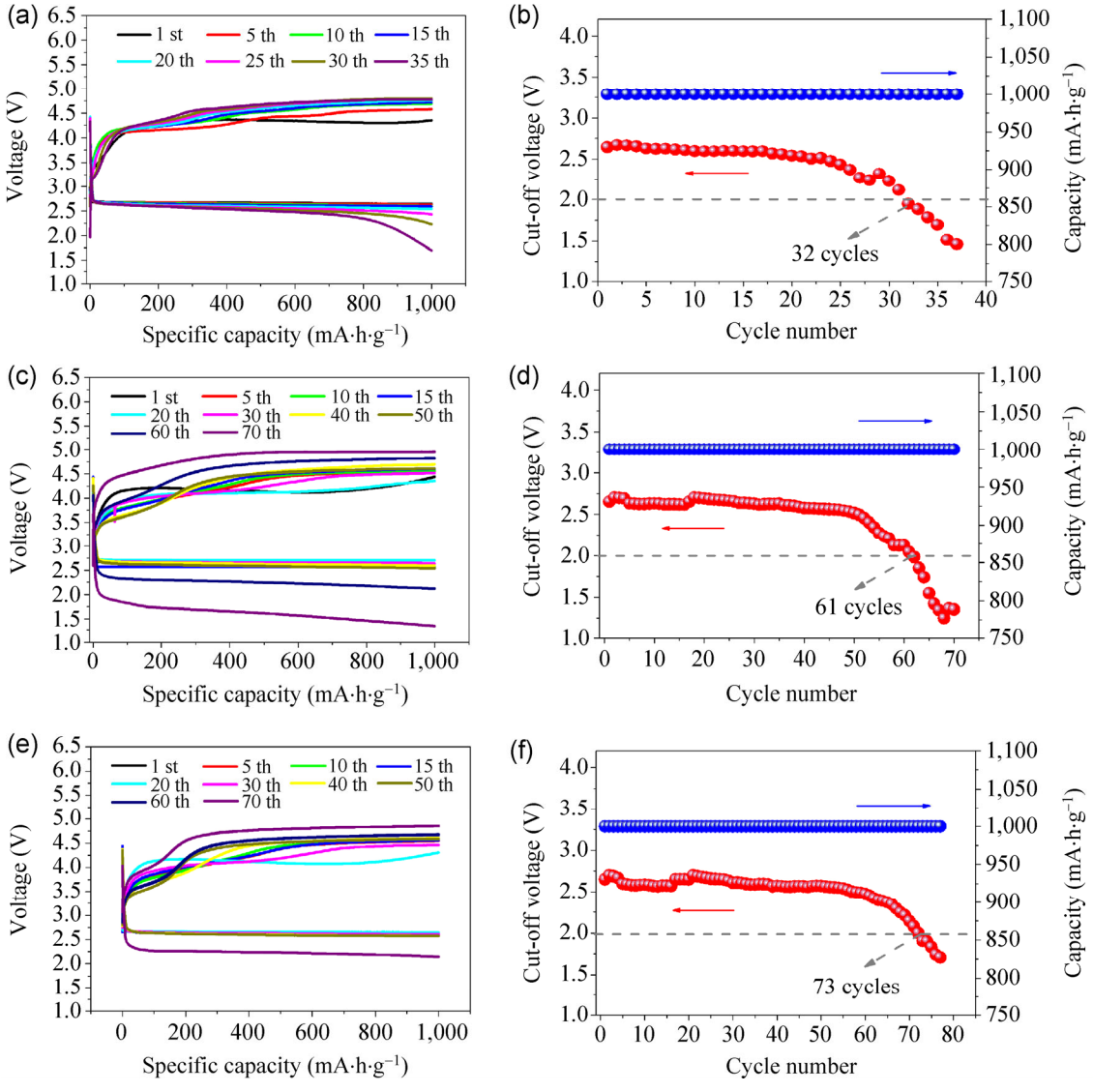

Figure 3 Discharge–charge curves of Li–O_2 cells with (a) SP, (c) Co_3O_4 NPs/SP, or (e) Co_3O_4 NWs/SP cathodes; (b), (d), and (f) are their cycling performances, respectively.

catalyst (73 cycles) significantly improved the cycling stability of the Li–O_2 cell, which further confirms the efficient catalytic activity of Co_3O_4 as well as the beneficial affect of the larger surface area of the Co_3O_4 NWs.

The morphology variation of the SP, Co_3O_4 NPs/SP or Co_3O_4 NWs/SP cathodes was then investigated. It was found that, after discharge, the classical toroidal discharge product was uniformly and fully distributed on the three cathodes (Figs. 4(b), 4(e), and 4(h)) [27–32]. Surprisingly, the particle size of the discharge products in the three cathodes was quite different (decreasing from 1,000 to 300 nm with addition of Co_3O_4 NPs or NWs). However, it should be noted that the discharge current density can also influence the morphology of Li_2O_2 [25]. To exclude this possibility, the same current density of 100 mA·g^{-1} was employed in this study. Therefore, the generation of smaller particles of the discharge product can reasonably be attributed to the addition of Co_3O_4. Theoretically, a discharge product with smaller particle size could provide a larger contact area with the conducting carbon electrode and electrolyte, and thus facilitate electron/Li^+ transfer, which should improve the electrochemical performance (vide supra). Furthermore, the crystallinity of the discharge product for these three cathodes was also

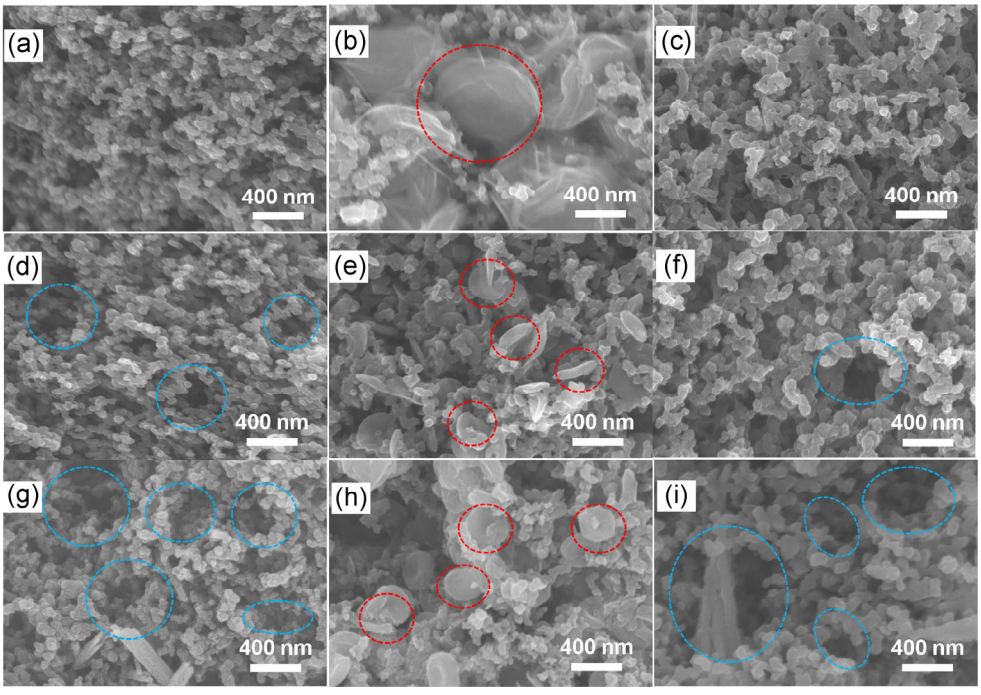

Figure 4 SEM images of the ((a), (d), and (g)) pristine, ((b), (e) and (h)) discharged, and ((c), (f), and (i)) recharged SP, Co_3O_4 NPs/SP, or Co_3O_4 NWs/SP cathodes.

different. As shown in Fig. S7 in the ESM, it was found that, with the addition of Co_3O_4 NPs or Co_3O_4 NWs, the crystallinity of the discharge product decreased. A discharge product with decreased crystallinity might have more defects, such as lithium vacancies, which could increase the ionic conductivity of Li_2O_2 [33]. Both the small particle size and decreased crystallinity could facilitate the decomposition of the discharge product during the charge process and thus improve the cycling performance of the Li–O_2 batteries. We suggest that the Co_3O_4 has a suitable oxygen binding energy, leading to stronger oxygen adsorption on the Co_3O_4 surface than on the carbon, which might facilitate the formation of poorly crystalline Li_2O_2. However, it should be noted that a detailed understanding of the decreasing particle size and crystallinity of the discharge product requires further study. Furthermore, the cathode structure could also contribute to the enhanced cycling performance. With the addition of Co_3O_4 NPs (Fig. 4(d)) or, especially, Co_3O_4 NWs (Fig. 4(g)), the cathodes become less compact compared to the pristine SP cathode (Fig. 4(a))—some macropores (the blue dotted line circles) appear, which still exist even in the subsequent recharged cathodes (Figs. 4(f) and 4(i)). These macropores offer ample space for accommodating the discharge product and favor reactant transfer, by avoiding cathode clogging, and thus improve the cycling performance. In this context, due to their hierarchical structure, the Co_3O_4 NWs can more effectively tailor the cathode structure compared to the zero-dimensional Co_3O_4 NPs. As a result, the cell with the Co_3O_4 NWs/SP cathode exhibits more stable cycling performance (Figs. 3(e) and 3(f)) than that with the Co_3O_4 NPs/SP cathode (Figs. 3(c) and 3(d)).

4 Conclusions

High surface area Co_3O_4 NWs with a chrysanthemum-like structure have been successfully synthesized via a novel hydrothermal and calcination method. When employed as bifunctional cathode catalysts for non-aqueous Li–O_2 batteries, superior electrochemical performance—including specific capacity, round-trip efficiency, and cycling stability—were obtained, which can be attributed to the high catalytic activity of Co_3O_4 as well as the high surface area and tailored structure of Co_3O_4 NWs.

Acknowledgements

This work is financially supported by the 100 Talents Programme of the Chinese Academy of Sciences, the National Program on Key Basic Research Project of China (973 Program, Grant No. 2012CB215500), the Foundation for Innovative Research Groups of the National Natural Science Foundation of China (Grant No. 20921002), the National Natural Science Foundation of China (Grant No. 21101147), and Jilin Province Science and Technology Development Program (Grant No. 201215141).

Electronic Supplementary Material: Supplementary material (characterization of the precursor and Co_3O_4 NPs, EIS spectra, and rate capability of Co_3O_4 NWs) is available in the online version of this article at http://dx.doi.org/10.1007/s12274-014-0689-3.

References

[1] Wang, Y. G.; He, P.; Zhou, H. S. A lithium–air capacitor–battery based on a hybrid electrolyte. *Energy Environ. Sci.* **2011**, *4*, 4994–4999.

[2] Abraham, K. M.; Jiang, Z. A polymer electrolyte-based rechargeable lithium/oxygen battery. *J. Electrochem. Soc.* **1996**, *143*, 1–5.

[3] Lu, Y. C.; Gasteiger, H. A.; Parent, M. C; Chiloyan, V.; Shao-Horn, Y. The influence of catalysts on discharge and charge voltages of rechargeable Li–oxygen batteries. *Electrochem. Solid-State Lett.* **2010**, *13*, A69–A72.

[4] Zheng, J. P.; Liang, R. Y.; Hendrickson, M.; Plichta, E. J. Theoretical energy density of Li–air batteries. *J. Electrochem. Soc*. **2008**, *155*, A432–A437.

[5] Ogasawara, T.; Débart, A.; Holzapfel, M.; Novák, P.; Bruce, P. G. Rechargeable Li_2O_2 electrode for lithium batteries. *J. Am. Chem. Soc.* **2006**, *128*, 1390–1393.

[6] Zhao, N.; Li, C. L.; Guo, X. X. Review of methods for improving the cyclic stability of Li–air batteries by controlling cathode reactions. *Energy Technol.* **2014**, *2*, 317–423

[7] Li, F. J.; Zhang, T.; Zhou, H. S. Challenges of non-aqueous Li–O_2 batteries: Electrolytes, catalysts, and anodes. *Energy Environ. Sci.* **2013**, *6*, 1125–1141.

[8] Xu, J. J.; Xu, D.; Wang, Z. L.; Wang, H. G.; Zhang, L. L; Zhang, X. B. Synthesis of perovskite-based porous $La_{0.75}Sr_{0.25}MnO_3$ nanotubes as a highly efficient electrocatalyst for rechargeable lithium–oxygen batteries. *Angew. Chem. Int. Ed.* **2013**, *52*, 3887–3890.

[9] Zhang, Z. A.; Zhou, G.; Chen, W.; Lai, Y. Q.; Li, J. Facile synthesisof Fe_2O_3 nanoflakes and their electrochemical properties for Li–air batteries. *ECS Electrochem. Lett.* **2014**, *3*, A8–A10.

[10] Black, R.; Lee, J. H.; Adams, B.; Mims, C. A.; Nazar, L. F. The role of catalysts and peroxide oxidation in lithium–oxygen batteries. *Angew. Chem. Int. Ed.* **2013**, *52*, 392–396.

[11] Ryu, W. H.; Yoon, T. H.; Song, S. H.; Jeon, S.; Park, Y. J.; Kim, I. D. Bifunctional composite catalysts using Co_3O_4 nanofibers immobilized on nonoxidized graphene nanoflakes for high capacity and long-cycle Li–O_2 batteries. *Nano Lett.* **2013**, *13*, 4190–4197.

[12] Zhang, L. L.; Zhang, X. B.; Wang, Z. L.; Xu, J. J.; Xu, D. Wang, L. M. High aspect ratio γ-MnOOH nanowires for high performance rechargeable nonaqueous lithium–oxygen batteries. *Chem. Commun.* **2012**, *48*, 7598–7600.

[13] Cao, Y.; Wei, Z. K.; He, J.; Zang, J.; Zhang, Q.; Zheng, M. S.; Dong, Q. F. α-MnO_2 nanorods grown *in situ* on graphene as catalysts for Li–O_2 batteries with excellent electrochemical performance. *Energy Environ. Sci.* **2012**, *5*, 9765–9768.

[14] Débart, A.; Bao, J. L.; Armstrong, G.; Bruce, P. G. An O_2 cathode for rechargeable lithium batteries: The effect of a catalyst. *J. Power Sources* **2007**, *174*, 1177–1182.

[15] Tüysüz, H.; Hwang, Y. J.; Khan, S. B.; Asiri, A. M.; Yang, P. D. Mesoporous Co_3O_4 as an electrocatalyst for water oxidation. *Nano Res.* **2013**, *6*, 47–54.

[16] Du, H. M, Jiao, L. F.; Wang, Q. H.; Yang, J. Q.; Guo, L. J.; Si, Y. C.; Wang, Y. J.; Yuan, H. T. Facile carbonaceous microsphere templated synthesis of Co_3O_4 hollow spheres and their electrochemical performance in supercapacitors. *Nano Res*. **2013**, *6*, 87–98.

[17] Wu, H.; Xu, M.; Wang, Y. C.; Zheng, G. F. Branched Co_3O_4/Fe_2O_3 nanowires as high capacity lithium-ion battery anodes. *Nano Res.* **2013**, *6*, 167–173.

[18] Su, D. W.; Dou, S. X.; Wang, G. X. Mesocrystal Co_3O_4 nanoplatelets as high capacity anode materials for Li-ion batteries. *Nano Res.* **2014**, *7*, 794–803.

[19] Kim, W. S.; Hwa, Y.; Kim, H. C.; Chio, J. H.; Sohn, H. J.; Hong, S. H. SnO_2@Co_3O_4 hollow nano-spheres for a Li-ion battery anode with extraordinary performance. *Nano Res.* **2014**, *7*, 1128–1136.

[20] Liu, Q. C.; Xu, J. J.; Chang, Z. W.; Zhang, X. B. Direct electrodeposition of cobalt oxide nanosheets on carbon paper as free-standing cathode for Li–O_2 battery. *J. Mater. Chem. A* **2014**, *2*, 6081–6085.

[21] Xu, J. J.; Wang, Z. L.; Xu, D.; Zhang L. L.; Zhang, X. B. Tailoring deposition and morphology of discharge products towards high-rate and long-life lithium–oxygen batteries. *Nat. Commun.* **2013**, *4*, 2438.

[22] Sun, B.; Huang X. D.; Chen, S. Q.; Munroe, P. R.; Wang, G. X. Porous graphene nanoarchitectures—An efficient catalyst for low charge-overpotential, long life and high capacity lithium–oxygen batteries. *Nano Lett.* **2014**, *14*, 3145–3152.

[23] Sun, B.; Liu, H.; Munroe, P.; Ahn, H.; Wang, G. X. Nanocomposites of CoO and a mesoporous carbon (CMK-3) as a high performance cathode catalyst for lithium–oxygen batteries. *Nano Res.* **2012**, *5*, 460–469.

[24] Dong, Y. M.; He, K.; Yin, L.; Zhang, A. M. A facile route to controlled synthesis of Co_3O_4 nanoparticles and their environmental catalytic properties. *Nanotechnology* **2007**, *18*, 435602.

[25] Adams, B. D.; Radtke, C.; Black, R.; Trudeau, M. L.; Zaghib, K.; Nazar, L. F. Current density dependence of peroxide formation in the Li–O_2 battery and its effect on charge. *Energy Environ. Sci.* **2013**, *6*, 1772–1778.

[26] Yilmaz, E.; Yogi, C.; Yamanaka, K.; Ohta, T.; Byon, H. R. Promoting formation of noncrystalline Li_2O_2 in the Li–O_2 battery with RuO_2 nanoparticles. *Nano Lett.* **2013**, *13*, 4679–4684.

[27] Gallant, B. M.; Kwabi, D. G.; Mitchell, R. R.; Zhou, J. G.; Thompson, C. V.; Shao-Horn, Y. Influence of Li_2O_2 morphology on oxygen reduction and evolution kinetics in Li–O_2 batteries. *Energy Environ. Sci.* **2013**, *6*, 2518–2528.

[28] Lu, J.; Lei, Y.; Lau, K. C.; Luo, X. Y.; Du, P.; Wen, J. G.; Assary, R. S.; Das, U.; Miller, D. J.; Elam, J. W.; et al. A nanostructured cathode architecture for low charge overpotential in lithium–oxygen batteries. *Nat. Commun.* **2013**, *4*, 2383

[29] Lu, Y. C.; Kwabi, D. G.; Yao, K. P. C.; Harding, J. R.; Zhou, J. G.; Zuin, L.; Shao-Horn, Y. The discharge rate capability of rechargeable Li–O_2 batteries. *Energy Environ. Sci.* **2011**, *4*, 2999–3007.

[30] Mitchell, R. R.; Gallant, B. M.; Shao-Horn, Y.; Thompson, C. V. Mechanisms of morphological evolution of Li_2O_2 particles during electrochemical growth. *J. Phys. Chem. Lett.* **2013**, *4*, 1060–1064.

[31] Fan, W. G.; Cui, Z. H.; Guo, X. X. Tracking formation and decomposition of abacus-ball-shaped lithium peroxides in Li–O_2 cells. *J. Phys. Chem. C* **2013**, *117*, 2623–2627.

[32] Jung, H. G.; Kim, H. S.; Park, J. B.; Oh, I. H.; Hassoun, J.; Yoon, C. S.; Scrosati, B.; Sun, Y. K. A transmission electron microscopy study of the electrochemical process of lithium–oxygen cells. *Nano Lett.* **2012**, *12*, 4333–4335.

[33] Tian, F.; Radin, M. D.; Siegel, D. J. Enhanced charge transport in amorphous Li_2O_2. *Chem. Mater.* **2014**, *26*, 2952–2959.